Neutron capture in ^{122,123,124}Te: Critical test for *s* process studies

K. Wisshak, F. Voss, and F. Käppeler
Kernforschungszentrum Karlsruhe, Institut für Kernphysik, D-7500 Karlsruhe, Germany

G. Reffo
Comitato Nazionale dell'Energia Nucleare e dell'Energie Alternative, I-40138 Bologna, Italy
(Received 4 November 1991)

The neutron capture cross sections of ^{122,123,124,125,126}Te were measured in the energy range from 10 to 200 keV at the Karlsruhe Van de Graaff accelerator using gold as a standard. Neutrons were produced via the ^{7}Li$(p,n)^{7}$Be reaction by bombarding metallic Li targets with a pulsed proton beam. Capture events were registered with the Karlsruhe 4π barium fluoride detector. Several sets of measurements were performed under different experimental conditions to study the systematic uncertainties in detail. The cross section ratios σ(Te)/σ(Au) were determined with an overall uncertainty of $\sim 1\%$. This is an improvement by about a factor of 5 compared to existing data. Maxwellian-averaged neutron capture cross sections were calculated for thermal energies between $kT=10$ and 100 keV by normalizing the cross section shape up to 600 keV neutron energy reported in literature to the present data. These stellar cross sections were used in an *s* process analysis. With the classical approach the abundances of the three *s* only isotopes ^{122,123,124}Te could be reproduced within the experimental uncertainties of $\sim 1\%$. The accuracy of the present data also allowed us to derive constraints for the existing stellar models with respect to the effective neutron density. Furthermore, the *p* process abundances for the tellurium isotopes are discussed.

PACS number(s): 25.40.Lw, 27.60.+j, 98.80.Ft

I. INTRODUCTION

The nucleosynthesis of the heavy elements by successive neutron captures in the so-called *s* process (*s* for slow neutron capture) is one of the topics in nuclear astrophysics that can be addressed in detail by laboratory experiments. The most important quantities in these investigations are the isotopic abundances, N_s, and the stellar neutron capture cross sections, $\langle\sigma\rangle$, averaged over a Maxwellian velocity distribution for a typical *s*-process temperature of $\sim 3\times 10^{8}$ K corresponding to thermal energies around $kT=30$ keV. Model descriptions [1] showed that the product $\langle\sigma\rangle N_s$ is a smooth function of mass number A.

Most important for characterizing the dependence of $\langle\sigma\rangle N_s(A)$ on mass are those isotopes which are produced only in the *s* process, since they are shielded from the *r* process (*r* for rapid neutron capture) by stable isobars. In these cases, the *s* process abundances, N_s, are identical with the solar abundances, $N_\odot$ (apart from minor *p* process contributions, see Sec. VII). The solar abundances are derived from the composition of primitive meteorites [2] and from the solar spectrum [3]. In certain mass regions it is possible to determine elemental abundance ratios with an uncertainty of $\sim 2\%$ (Refs. [4,5]). Of special interest in *s*-process studies are those eight elements (Kr, Sr, Te, Xe, Ba, Sm, Gd, Os) with two or three *s* only isotopes, since the abundance ratios of these isotopes are simply the isotopic ratios that are known with typical uncertainties of 0.1% (Ref. [6]). Therefore, these examples represent the most sensitive probes for details in the *s* process environment.

Information on the physical conditions during the *s* process, e.g., neutron density, temperature, and electron density, can be deduced from the analysis of branchings in the *s*-process path [1]. The branchings result from the competition between neutron capture and beta decay whenever an unstable isotope is encountered by the *s*-process path and that beta decay rate, $\lambda_\beta=\ln 2/t_{1/2}$, is comparable to its neutron capture rate, $\lambda_n=n_n v_T\langle\sigma\rangle$. In these expressions, $t_{1/2}$ is the half-life, n_n the *s*-process neutron density, v_T the mean thermal neutron velocity, and $\langle\sigma\rangle$ the stellar neutron capture cross section. The competition between beta decay and neutron capture defines the branching factor $f_n=\lambda_n/(\lambda_n+\lambda_\beta)$ for the *s*-process flow. The branching factor depends on the neutron density, n_n, and/or on temperature, T, or mass density, ρ, if the beta decay half-lives are sensitive to the stellar conditions. Stringent constraints on these parameters can be obtained from branchings that are defined by two *s*-only isotopes of the same element. The six branchings of this type are compiled in Table I and are illustrated in Fig. 1 by the example of the tellurium isotopes. Branchings at ^{121}Sn and ^{122}Sb cause part of the *s*-process flow to bypass ^{122}Te and ^{123}Te. In first approximation, the effect of these branchings is expressed by

$$1-f_n\cong\langle\sigma\rangle N_s(^{122}\mathrm{Te})/\langle\sigma\rangle N_s(^{124}\mathrm{Te})\ .$$

The uncertainty of this ratio is completely determined by the uncertainty of the cross sections. In a recent measurement by Macklin and Winters [7], an uncertainty of $\pm 5\%$ was obtained. Since f_n is expected to range between 0.01 and 0.05 according to estimates with the clas-

TABLE I. Branchings in the *s*-process path that are defined by two *s*-only isotopes of the same element.

s-only isotopes	Branching point	Branching factor f_n	Sensitive physical parameter
^{80,82}Kr	^{79}Se	0.50±0.12	temperature
^{122,123,124}Te	^{121}Sn,^{122}Sb	0.01±0.05[a]	neutron density
^{128,130}Xe	^{127}Te,^{128}I	0.01±0.25[a]	electron density, xenon abundance
^{134,136}Ba	^{133}Xe,^{134}Cs	0.02±0.15[a]	temperature and neutron density
^{148,150}Sm	^{147}Nd,^{147}Pm,^{148}Pm	0.10±0.05	neutron density
^{152,154}Gd	^{151}Sm,^{152}Eu	0.95±0.05	electron density

[a]Estimates from classical model much smaller than current experimental uncertainty.

sical approach and by stellar models, considerably more accurate cross sections are required for a quantitative analysis of these branchings.

A similar example is the branching at $A=147$, 148, which is defined by the two *s*-only isotopes ^{148}Sm and ^{150}Sm. This case is most suited for the determination of the neutron density, n_n. In a careful experiment [8] using a conventional technique the cross section ratio was determined with an uncertainty of ~4%. In the branching analysis, this uncertainty represents the dominant contribution to the ±40% uncertainty of the deduced neutron density. Hence, also for this branching a significant improvement can be expected from more accurate cross sections.

The aim of the present experiment is to apply a new method, which allows to determine cross section ratios with an uncertainty of ~1%. With such data on hand, it will be possible to improve our knowledge on the $\langle\sigma\rangle N_s(A)$ curve, and to check on the one percent level the prediction of the classical *s*-process model of a "local approximation," i.e., that the product $\langle\sigma\rangle N_s$ is constant for neighboring isotopes. Moreover, these data are the prerequisite for detailed analyses of the branchings listed in Table I, which will lead to significantly improved parameters for the physical conditions during the *s* process. This information will then allow us to improve the constraints for stellar models.

The most interesting candidates to start with are the isotopes of tellurium. Tellurium is the only element in nature with three *s*-only isotopes (see Fig. 1). From the classical model a very weak branching is predicted. Therefore, tellurium provides the only possibility for checking the accuracy of the local approximation for a chain of three neighboring isotopes. The unique fact that one of the *s*-only isotopes has an odd mass number and thus is not produced by the *p* process (see Sec. VII) even allows the exclusion of the possibility that a weak branching is masked by a corresponding *p*-process contribution, an ambiguity that has to be discussed for all other branchings. In addition, the data are expected to yield an upper limit for the neutron density as a constraint for current stellar models, and to allow for an estimate of the *p*-process contribution to the even tellurium isotopes.

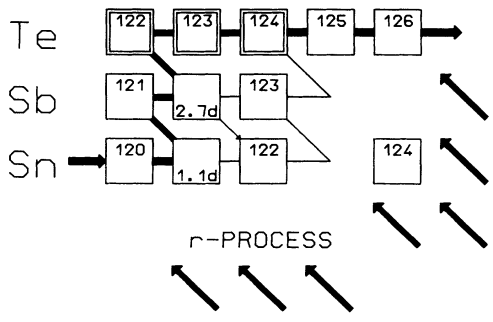

FIG. 1. The *s*-process path in the region of the tellurium isotopes. The *s*-only isotopes ^{122,123,124}Te are shielded from the *r* process by the stable isobars ^{122,124}Sn and ^{123}Sb. The unstable nuclei ^{121}Sn and ^{122}Sb are possible branching points.

In the following, we describe the experiment and data evaluation in Secs. II and III. The differential cross sections are presented in Sec. IV, while the uncertainties are discussed in Sec. V. Section VI is devoted to the determination of stellar cross sections, and the implications for the classical *s*-process approach are given in Sec. VII. A detailed discussion of the consequences for current stellar models will be the topic of a forthcoming publication.

II. EXPERIMENT

A. Experimental method

The neutron capture cross sections of the tellurium isotopes 122 to 126 were measured in the energy range from 10 to 200 keV using gold as a standard. The experimental method has been published in detail in Refs. [9] and [10]. Therefore only the essential features are presented here with emphasis on the peculiarities of the present measurement and on the changes and improvements that were introduced since our first experiment on Nb, Ta, and Rh (Ref. [10]). Neutrons were produced via the ^{7}Li$(p,n)^7$Be reaction by bombarding metallic Li targets with the pulsed proton beam of the Karlsruhe 3.75 MV Van de Graaff accelerator. The neutron energy is determined by time of flight (TOF), the samples being located at a flight path of 78 cm. The important parameters of the accelerator are pulse width ~1 ns, repetition rate 250 kHz, and average beam current 1.5–2 μA.

The neutron beam was collimated to 25 mm diameter at the sample position. The neutron flight path through collimator and detector was evacuated in order to eliminate background from neutrons scattered in the air. Since rather small sample masses are used in the present

experiment, the scattering background due to the 50 cm flight path in air through the detector (see below) would have been comparable with the scattering effect of the samples. Two thin stainless steel tubes closed by 20 μm thick Kapton foils were installed along the flight path leaving only a gap of $\sim$1 cm for the samples. The central part of the collimator was evacuated, too.

In three different runs, the energy of the proton beam was adjusted 10, 30, and 100 keV above the reaction threshold of the ^{7}Li$(p,n)^7$Be reaction at 1.881 MeV. This yields continuous neutron spectra in the energy range of interest for *s*-process studies, i.e., 10–70, 3–100, and 3–200 keV, respectively. The use of different spectra allowed us to optimize the signal to background ratio in different neutron energy regions (see Sec. III). The thickness of the metallic lithium targets was chosen so as to reduce the energy of the proton beam just below the threshold of the (p,n) reaction in order to minimize the intensity of gamma rays produced by inelastic scattering (E_γ=478 keV) on ^{7}Li, and by the ^{7}Li(p,γ) reaction (E_γ=16 and 19 MeV). For the maximum energy loss of 100 keV, a lithium layer of $\sim$1 mg/cm^2 was sufficient.

The Karlsruhe 4π barium fluoride detector was used for the registration of capture gamma-ray cascades. This detector (a comprehensive description is given in Ref. [9]) consists of 42 hexagonal and pentagonal crystals forming a spherical shell of BaF_2 with 10 cm inner radius and 15 cm thickness. It is characterized by a resolution in gamma-ray energy of 7% at 2.5 MeV, a time resolution of 500 ps, and a peak efficiency of 90% at 1 MeV. Capture events are registered with $\sim$95% probability.

The main advantages of this experimental method are the following: The entire capture cascade is detected with good energy resolution. Thus, ambiguities in the detection efficiency due to different cascade multiplicities are avoided. Capture events are concentrated around the binding energies of the respective isotopes ($\sim$6 MeV) and thus well separated from most gamma-ray background ($<$3 MeV). Background due to capture of sample scattered neutrons appears mainly at $\sim$9 MeV (see Sec. III). The subdivision of the detector into many individual modules allows for a further separation of capture events and background by the event multiplicity. The short primary flight path and the inner radius of the detector guarantees that part of the TOF spectra is completely undisturbed by background from sample scattered neutrons (see Sec. III). This range with optimum signal to background ratio can be used to normalize the cross section. The high detection efficiency allows the use of small samples avoiding large multiple scattering corrections. Finally, the ^{7}Li(p,n) reaction yields neutrons exactly and exclusively in the range of interest for *s*-process studies.

B. Samples

Metallic, isotopically enriched samples have been used. The relevant parameters of the eight samples mounted simultaneously in the sample changer are compiled in Table II. The tellurium samples were pellets pressed from metal powder. Their weight was selected according to the expected cross sections in order to obtain similar capture yields per sample. The sample masses of the main isotopes, ^{122,123,124}Te, are lower in weight by factors of 3 to 14 compared to the samples used by Macklin and Winters [7]. Hence, sample-related uncertainties, i.e., for multiple scattering and self-shielding corrections, are significantly reduced. The heavier isotopes, ^{125}Te and ^{126}Te, were included in the measurement to correct the data of the other samples for isotopic impurities.

The exact characterization of the sample is a severe problem for accurate cross section measurements [11]. This was particularly difficult in the case of tellurium, due to the oxygen affinity of this element. Another problem is a possible contamination with hydrogen in the form of water or of a hydride [12]. Therefore, the material was carefully analyzed to detect contaminations of these two elements. The sample material was stored in a glove box under argon atmosphere, the samples were welded into thin polyethylene foils during the experiment to avoid oxygen absorption, and their weight was controlled before and after the measurement. These precautions were necessary since dummy samples from natural tellurium powder showed an increase in weight of 0.3% per week when stored in air. The unwanted hydrogen introduced in this way results in a transmission of the foil of 0.9984, and in a slightly moderated neutron flux at the position of the sample. However, this effect cancels out to a large extent in the present experiment since samples

TABLE II. Compilation of relevant sample data.

Sample[a]	Thickness (mm)	Thickness[b] (10^{-3} atom/b)	Weight (g)	Oxygen content (%)[c]	Impurity[d] (%)[c]	Neutron binding energy (MeV)
(1) Au	0.8	4.3427	1.115 56	0	$<$0.01	6.513
(2) Graphite	1.3	10.579	0.165 72	0		
(3) ^{122}Te	2.4	6.5889	1.059 07	0.72	$<$0.03	6.933
(4) ^{123}Te	1.2	2.2831	0.417 94	12.1	$<$0.03	9.424
(5) ^{124}Te	5.0	13.181	2.155 49	0.98	$<$0.03	6.571
(6) ^{125}Te	2.2	5.5059	0.921 25	2.48	$<$0.02	9.120
(7) No sample						
(8) ^{126}Te	4.0	10.257	3.917 42	3.17	$<$0.02	6.290

[a]Samples of 10 mm diameter except ^{126}Te (15 mm diameter).
[b]For samples 3–8 sum of all Te isotopes (oxygen not included).
[c]% of weight.
[d]Impurity of other elements except oxygen.

and reference sample are affected in the same way due to their similar cross section shapes.

The sample material was checked via gas analysis of solids using the method of vacuum hot extraction. For this purpose, 10 mg powder was molten under vacuum in a graphite container together with a bath material (2 g ultrapure Sn) at a temperature of 2300 °C. The tellurium metal forms on alloys with the bath material. Hydrogen, either in the form of a hydride or absorbed as water, is released into the gaseous phase. The same happens to oxygen impurities, which react with the graphite to form CO. The hydrogen is detected in the gaseous phase by measuring the heat conductivity and the CO by infrared absorption. The apparatus is calibrated by gases with well defined composition. The method was optimized and checked using natural tellurium oxide. Two (and in case of ^{123}Te three) independent measurements have been performed for each sample material to prove the reproducibility of the method and the homogeneity of the powder. The results—compiled in Table II—showed that the "metallic" ^{123}Te powder supplied by ORNL was strongly oxidized. The other isotopes, which we had on loan from the USSR, were better defined, but in any case, data analysis simply adopting the specified metallicity of the suppliers would have led to disasterous errors in the cross sections. Hydrogen was not detected in the sample material. It should be stressed that such problems with unexpected sample impurities may well be one of the reasons for the discrepancies in neutral capture cross section measurements that can be found in literature.

The isotopic composition was redetermined at KfK with two thermion mass separators, one with a 90° magnetic sector field, and the other with an electric quadrupole analyzer. The results are compiled in Table III together with the data provided by the suppliers. In general good agreement is found, the only significant differences being observed for the isotopes 122 and 123 in the ^{122}Te sample (see Sec. V).

The diameter of the samples was 10 mm. In case of ^{126}Te, the sample mass of 4 g made it necessary to increase the diameter to 15 mm. As can be seen from Table II, the thickness of some samples is relatively large and the transmission is only 0.92. Since accurate data for the total cross section of the tellurium isotopes were not available from literature, the spectra measured with the neutron monitor at 260 cm flight path did not allow us to check the normalization of the neutron flux as in our first measurement (Ref. [10]).

C. Measurements

The samples were moved cyclically into the measuring position by a computer controlled sample changer. The data acquisition time per sample was about 10 min, and the time for completion of one cycle about 1.5 h. From each event, a 64 bit word was recorded on magnetic tape containing the sum energy and TOF information together with 42 bits indicating those detector modules that have contributed. As mentioned above, three measurements for each sample were performed using neutron spectra with 200, 100, and 70 keV maximum energy, respectively. In one run, the threshold in the sum energy spectrum was lowered to 1.9 MeV, while in the other runs it was fixed at 2.4 MeV. This threshold determines the recorded event rate, which was ~1 kHz for the lower and 500 Hz for the higher threshold. In total, ~200 high density tapes of data containing roughly 30 Gbyte of information were recorded during this experiment. The spectra of the two neutron monitor detectors were stored on disk.

III. DATA EVALUATION

The procedures of data evaluation have been described in detail in Ref. [10]. For the present experiment, the details of data evaluation, calculation of correction factors, and the results of individual runs and evaluation methods are given in Ref. [13]. All events stored on magnetic tape were sorted into two-dimensional sum energy versus TOF spectra according to event multiplicities (evaluation 1). In evaluation 2, this procedure was repeated by rejecting those events for which only neighboring detector modules contributed to the sum energy signal in order to reduce background from the natural radioactivity of the BaF_2 crystals and from capture of scattered neutrons in the scintillator material. These two-dimensional spectra were normalized to equal neutron flux using the count rate from the lithium glass monitor, which was located close to the neutron target; these normalization factors are in general well below 1% (see Sec. V). In the next step, the spectra measured without sample were subtracted to re-

TABLE III. Comparison of the isotopic enrichments of the tellurium samples (%) as quoted by the suppliers and measured at KfK.

	Isotope								
Sample	120	122	123	124	125	126	128	130	
^{122}Te	<0.01	91.2	1.23	1.91	0.80	1.57	1.91	1.38	USSR
	<0.01	91.86	0.61	1.77	0.78	1.58	1.98	1.42	KfK
^{123}Te	<0.02	0.54	89.39	1.59	1.24	2.72	2.53	1.99	ORNL
	<0.01	0.48	89.58	1.52	1.24	2.68	2.51	1.99	KfK
^{124}Te	<0.002	0.07	0.07	92.4	4.06	1.59	1.06	0.75	USSR
	<0.01	<0.2	<0.1	92.61	4.03	1.55	1.07	0.74	KfK
^{125}Te	<0.006	<0.006	<0.006	0.88	93.9	3.61	1.06	0.55	USSR
	<0.01	<0.05	<0.03	0.90	93.88	3.55	1.07	0.60	KfK
^{128}Te	<0.026	<0.026	0.08	0.09	0.16	98.4	0.93	0.34	USSR
	<0.01	<0.02	<0.01	0.07	0.17	98.58	0.85	0.34	KfK

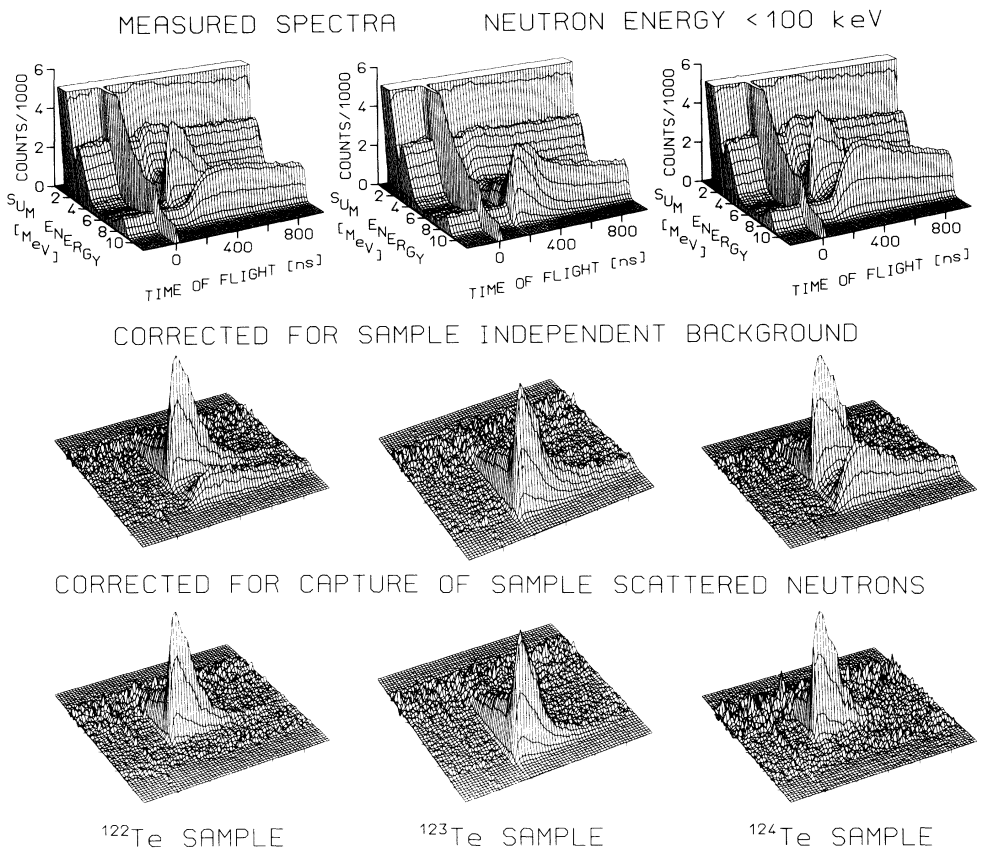

FIG. 2. The different steps of background subtraction in the two-dimensional sum energy vs TOF spectra. Events with multiplicity $m > 2$ are shown for the s-only tellurium isotopes measured in the run with 100 keV maximum neutron energy. (The original resolution of 128×2048 channels was compressed in the plots into 64×64 channels.)

move the sample-independent background. The remaining time-independent background was determined at very long flight times (~ 3.9 μs), where no time-correlated events are expected. Examples of these procedures are shown in Fig. 2, where the two-dimensional spectra of the run with 100 keV maximum neutron energy containing all events with multiplicity > 2 are given.

At this point, the spectra contain only events that are correlated with the sample. The next correction to be made was for isotopic impurities. In contrast to neutron capture experiments without resolution in gamma-ray energy [8], the contribution to isotopic impurities has to be eliminated from the measured spectra before evaluating the correction for scattered neutrons or determining a capture yield. This is important, since the respective events are located at different sum energies. Therefore, the spectra of the impurity isotopes were subtracted after normalization such that they account for their respective isotropic abundance. The coefficients are compiled in Table IV. The isotopes ^{128}Te and ^{130}Te, not covered by the present experiment, were treated as ^{126}Te, since this isotope has about the same binding energy. The cross section ratio was assumed to be energy independent and to scale as 1:0.5:0.2 for ^{126}Te:^{128}Te:^{130}Te according to Ref. [14]. The impurities of these isotopes are in the percent range and their cross sections are small. Therefore, this assumption does not affect the results. The worst case is ^{124}Te, where according to Table IV the corrected spectrum is calculated by

$$^{124}\mathrm{Te}_{\mathrm{corr}} = {}^{124}\mathrm{Te}_{\mathrm{meas}} - 0.1027\,{}^{125}\mathrm{Te}_{\mathrm{meas}} - 0.0118\,{}^{126}\mathrm{Te}_{\mathrm{meas}} .$$

As the sample masses are selected to give equal capture

TABLE IV. Matrix for the isotopic correction (%), using the approximation $\sigma(^{128}\mathrm{Te}) = 0.5\sigma(^{126}\mathrm{Te})$ and $\sigma(^{130}\mathrm{Te}) = 0.2\sigma(^{126}\mathrm{Te})$.

Corrected spectrum	Measured spectrum ^{122}Te	^{123}Te	^{124}Te	^{125}Te	^{126}Te	Corrected sample thickness (10^{-3} atom/b)
^{122}Te	100	−1.966	−0.9450	−0.8805	−0.7932	6.0523
^{123}Te	−0.1817	100	−0.2799	−0.5137	−0.4223	2.0451
^{124}Te			100	−10.2678	−1.1833	12.2016
^{125}Te			−0.4050	100	−1.0078	5.1664
^{126}Te			−0.1297	−0.7451	100	10.1601

yield, this relation seems to imply that the ^{124}Te yield is reduced by ~10%. Actually, the reduction is less than 4% as most of the count rate in the ^{125}Te spectrum is located near the binding energy of 9 MeV, a region that is not used for evaluation of the ^{124}Te cross section at all (binding energy 6.6 MeV).

In the corrected spectrum calculated, e.g., for ^{122}Te, from the five measured spectra and using the matrix elements given in Table IV, not only the isotopic impurities of ^{123}Te to ^{126}Te are eliminated, but also the effect of the main isotope is reduced. This is because the spectra measured with the other samples contain ^{122}Te as an impurity. In the final analysis, this was considered by a corrected sample thickness, which is given in the last column of Table IV.

After the correction for isotopic impurities, the background due to capture of sample scattered neutrons was removed from the spectra by means of the data measured with the carbon sample. The scattered neutrons are captured mainly in the barium isotopes of the scintillator. This is shown in Fig. 3, where the sum energy of the events recorded with the graphite sample is plotted. The binding energy of the even tellurium isotopes being below 7 MeV, capture events in ^{135,137}Ba are well separated by their sum energy from the true capture events in the sample. The energy range from 8 to 10 MeV (shaded box on the right in Fig. 3) is used to normalize the carbon spectrum for subtraction of the sample scattered neutron background. This normalization is calculated dependent on the TOF, which is very important for the accuracy of the experimental method. After subtraction, the spectra contain true capture events only (lower part of Fig. 2), and can be used to determine the cross section.

For the odd tellurium isotopes, this procedure is not applicable since their binding energy is ~9 MeV. In this case, the correction for sample scattered neutrons had to be normalized at the peak due to capture in ^{134}Ba and ^{136}Ba (see shaded box on the left in Fig. 3), which was integrated for several TOF intervals. This method, however, leads to systematic uncertainties at very low neutron energies because of the reduced signal-to-background ratio. For the odd isotopes the cross section was, therefore, evaluated only above 15 keV neutron energy.

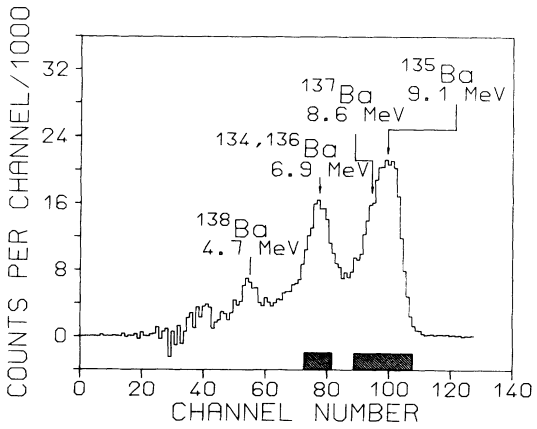

FIG. 3. Sum energy spectrum measured with the graphite sample, showing capture events in the different barium isotopes of the scintillator. The shaded boxes indicate the regions that were used to normalize the corresponding backgrounds for the odd (left) and even (right) tellurium isotopes, respectively.

In Fig. 4, the TOF spectra of the ^{122}Te sample are projected from the two-dimensional data using only the sum energy region with optimum signal to background ratio near the binding energy (see below). The background due to capture of sample scattered neutrons is shown separately. The data are given for the three experimental runs with 200, 100, and 70 keV maximum neutron energy, illustrating that the signal to background ratio at 30 keV increases from 4.0 to 5.7 and 7.4 in these cases, respectively. At low neutron energies, the signal to background ratio is rapidly decreasing. In view of the comparably small cross sections of the isotopes investigated here, it is, therefore, not possible to extend the evaluation below 10 keV with sufficient statistical accuracy.

After background subtraction, the TOF spectra shown in Fig. 4 were used to determine the shape of the cross section. For normalization, the two-dimensional spectra were projected onto the sum energy axis in the region of optimum signal to background ratio as indicated by shad-

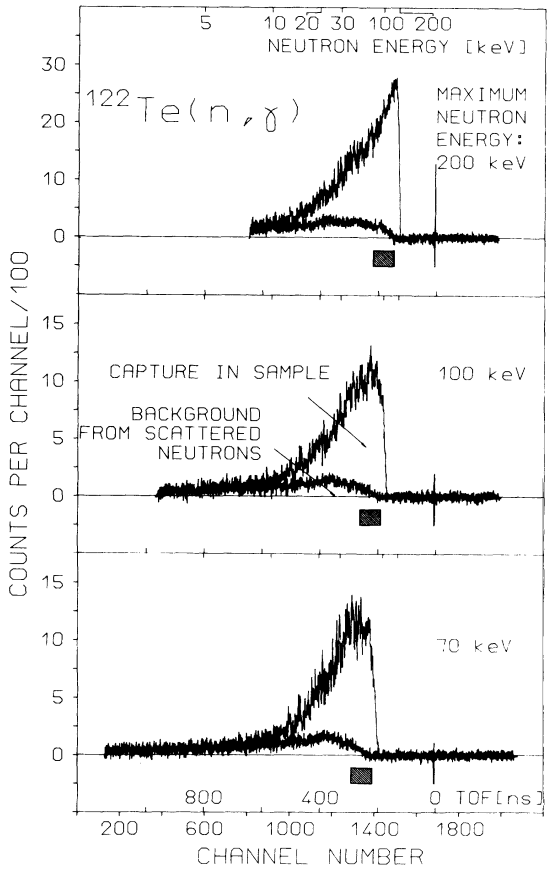

FIG. 4. TOF spectra measured with the ^{122}Te sample in runs with different maximum neutron energy. The background due to capture of sample scattered neutrons is shown separately. The signal to background ratio at 30 keV increases from 4.0 to 5.7 and 7.4 by lowering the maximum neutron energy. The TOF region used for the absolute normalization of the cross section is shown by the shaded box.

ed boxes in Fig. 4. The result is shown in Fig. 5 where the events with multiplicity >2 are plotted for all isotopes.

In Fig. 6, the sum energy spectra of ^{122}Te and ^{123}Te are shown as a function of the detector multiplicity. A multiplicity ≥ 5 is observed for $\sim 40\%$ of the events in the even and for $\geq 60\%$ in the odd tellurium isotopes. Gamma-ray background affects mainly the spectra with multiplicity 1 and 2 below ~ 4 MeV (channel number 45) giving rise to large statistical fluctuations. The figure demonstrates the potential of the detector as a multiplicity filter which separates capture events with high multiplicity from gamma-ray background with low multiplicity.

The cross section ratio of isotope X relative to the gold standard is then

$$\frac{\sigma_i(X)}{\sigma_i(\mathrm{Au})} = \frac{Z_i(X)}{Z_i(\mathrm{Au})} \frac{\sum Z(\mathrm{Au})}{\sum Z(X)} \frac{\sum E(X)}{\sum E(\mathrm{Au})} \frac{m(\mathrm{Au})}{m(X)} F_1 F_2 \,. \tag{1}$$

In this relation, Z_i is the count rate in channel i of the TOF spectrum, $\sum Z$ is the integral TOF count rate in the interval used for normalization (see Fig. 4), $\sum E$ is the total count rate in the sum energy spectrum for all multiplicities summed over the normalization interval (see Fig. 6), and m is the sample thickness in atoms/b. The correction factor F_1 is the ratio of the capture events below the threshold for sample and reference sample (Table V), and F_2 the respective ratio of the multiple scattering corrections (Table VI).

The fraction of unobserved capture events, f and the correction factor F_1, were calculated as described in detail in Ref. [10]. For this purpose, two items of information are necessary: the individual neutron capture cascades and their relative contribution to the total capture cross section as well as the detector efficiency for monoenergetic gamma rays in the energy range up to 10 MeV.

The capture cascades and capture gamma-ray spectra of the involved isotopes have been calculated according to the statistical and optical model [15], details being compiled in Ref. [13]. The 20 most probable cascades yield 25–35 % of the cross section, but up to 1000 were used in evaluating F_1 in order to cover 95% of the cross section. The average multiplicity of the cascades ranges for the different isotopes from 3.2 to 3.8.

The efficiency of a BaF_2 shell for monoenergetic gamma rays was calculated in Ref. [16] with different assumptions for multiple Compton events, resulting in an optimistic and a pessimistic estimate for the peak efficiency, SW(MAX) and SW(MIN). The data given in Ref. [10] were used to calculate the fraction f of unobserved capture events (see Table V). In the actual measurements, we used a threshold in the sum energy of 1.9 MeV in one run and of 2.4 MeV in the two others. Accordingly, the efficiency of the detector was 97–98 % for the odd and 93–95 % for the even isotopes. It has to be noted that for the present experimental method it is not necessary to know the absolute efficiency of the detector, which depends on the efficiency for monoenergetic gamma rays. As can be seen from Table V, differences of the order of 1% are observed for the different assumptions SW(MAX) and SW(MIN). Since sample and standard are measured with the same detector, the final correction factors F_1 are quite insensitive to the assumed detector efficiency. For the even isotopes, which are close in binding energy to

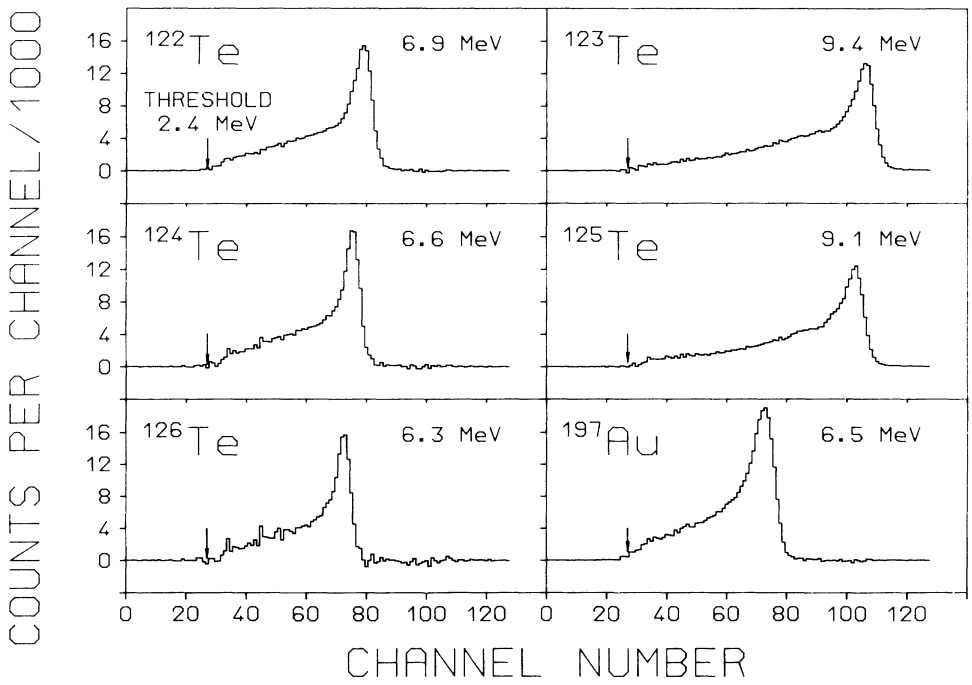

FIG. 5. Sum energy spectra of all isotopes measured in the run with 200 keV maximum neutron energy containing all events with multiplicity >2. These spectra were obtained by projection of the two-dimensional spectra in the TOF region below the maximum neutron energy as indicated for the ^{122}Te sample in Fig. 4.

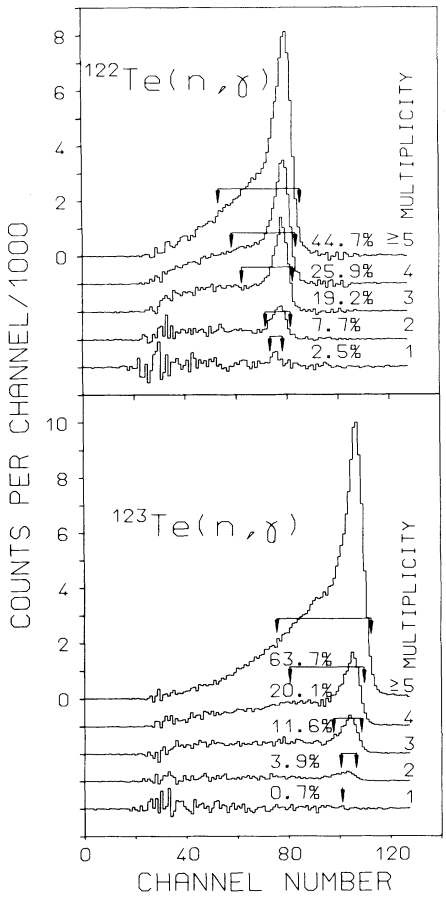

FIG. 6. Sum energy spectra from ^{122}Te and ^{123}Te in dependence of detector multiplicity (the same data as shown in Fig. 5). The regions used to determine the cross section shape are indicated by arrows. The relative intensity of the capture events is given in percent.

the gold standard, the correction is very small and only for the odd isotopes differences in efficiency of several percent are found.

In Fig. 7, the calculated sum energy spectra are shown separately for the two different assumptions of the detector efficiency. Comparison with the experimental results given in Fig. 5 demonstrates that they are indeed between these two extremes.

The correction for multiple scattering and self-shielding in the sample was calculated by the SESH code [17]. Recently, the code was changed by the author to consider the more accurate formula for the level density as described in Ref. [10]. The parameter of nuclear temperature was replaced by the pairing energy Δ which was taken from Ref. [18]. Now, the level spacing of p and d waves is calculated by the program. The main problem is to find sets of parameters that reproduce not only the capture cross section but, in addition, the total cross section of each isotope as well. It turned out, that experimental results on the total cross section were not available in the energy range considered. Data were published only above 200 keV in the work of Musaelyan and Skorkin [19]. Therefore, the calculations were made in three different ways in order to find the most reliable results and to study the sensitivity on the input parameters.

In the first calculation, we started from the parameters given by Mughabghab [20]. These data were changed such that the total cross section of the Joint Evaluated File (JEF) evaluation [21] was reproduced within an uncertainty of $\sim$3% and the capture cross sections of Macklin and Winters [7] within $\sim$10%. The respective input parameters as well as the results for the total cross sections are compiled in Ref. [13]. In the second step, a detailed resonance analysis was performed using the possibilities of the Bologna group, i.e., analysis of the cumulative number of neutron width distributions, of the cu-

TABLE V. Calculated fraction of unobserved capture events, f (%), and the corresponding correction factors, F_1, for the cross section ratios.

Sample	Threshold in sum energy (MeV) 1.5	1.9	2.0	2.4	2.5	Assumption for gamma-ray efficiency
Solid angle 94%, gamma-ray threshold 50 keV						
f(Au)	3.66		5.25		7.78	SW(MAX)
f(^{122}Te)	3.07		5.22		6.88	
f(^{123}Te)	1.27		1.89		3.30	
f(^{124}Te)	3.15		5.10		6.93	
f(^{125}Te)	1.00		1.48		2.27	
f(^{126}Te)	3.16		6.72		8.85	
f(Au)	4.08		6.19		8.99	SW(MIN)
f(^{122}Te)	3.63		5.89		8.95	
f(^{123}Te)	1.48		2.50		3.81	
f(^{124}Te)	3.70		5.87		8.40	
f(^{125}Te)	1.14		1.82		2.63	
f(^{126}Te)	4.02		7.45		9.93	
F_1(^{122}Te/Au)	0.995	0.997	0.998	0.996	0.995	$\frac{1}{2}$SW(MAX)
F_1(^{123}Te/Au)	0.975	0.967	0.964	0.953	0.950	$+\frac{1}{2}$SW(MIN)
F_1(^{124}Te/Au)	0.996	0.997	0.998	0.993	0.992	
F_1(^{125}Te/Au)	0.971	0.962	0.959	0.943	0.939	
F_1(^{126}Te/Au)	0.997	1.010	1.015	1.012	1.011	

TABLE VI. Correction factors for neutron multiple scattering and self-shielding, MS. The correction for the cross section ratio is given by $F_2 = \mathrm{MS(Au)/MS}(X)$.

Energy range (keV)	MS					
	Au	^{122}Te	^{123}Te	^{124}Te	^{125}Te	^{126}Te
5–10	0.997	0.952	0.997	0.933	0.965	0.960
10–15	1.020	0.975	1.007	0.950	0.986	0.968
15–20	1.031	0.985	1.009	0.956	0.995	0.972
20–30	1.037	0.991	1.010	0.961	1.002	0.975
30–40	1.038	0.995	1.011	0.967	1.005	0.976
40–60	1.036	0.998	1.010	0.974	1.007	0.979
60–80	1.034	1.000	1.010	0.979	1.008	0.983
80–100	1.031	1.002	1.010	0.983	1.008	0.985
100–120	1.029	1.002	1.009	0.986	1.008	0.988
120–150	1.026	1.003	1.009	0.988	1.009	0.991
150–200	1.023	1.003	1.008	0.990	1.009	0.995

mulative number of resonances, of the reduced neutron widths, the reduced neutron width sampling analysis, the truncated Porter-Thomas distribution, and the missing level estimator method. These studies led to a recommended set of parameters [13] which gave significantly larger total cross sections. This input was only slightly modified in order to reproduce the capture cross sections. Finally, the total cross sections were measured for the *s*-only isotopes in the energy range from 10 to 80 keV in a separate experiment [22] together with the shape of the capture cross section which was determined down to 1 keV. In this experiment, good agreement was found with the JEF data for ^{122}Te and ^{124}Te, while for ^{123}Te the cross section was significantly larger. Therefore, a third calculation was performed for this isotope increasing the S_0 strength function. In case of ^{123}Te, oxygen was included in the calculation. The contamination of 12.1% in weight (see Table II) leads to a contribution of 1.06 oxygen atoms per tellurium atom, which causes a significant increase of the total cross section. The correction factors MS(X) adopted in the final evaluation are compiled in Table VI; the results for the individual calculations which are necessary to estimate the uncertainty of this correction can be found in Ref. [13].

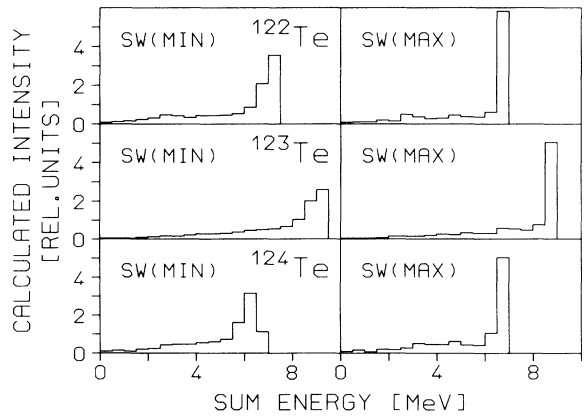

FIG. 7. Calculated sum energy spectra of the 4π BaF_2 detector as obtained under different assumptions on the detector efficiency. These spectra were used to derive the correction F_1 for unobserved capture events.

The comparatively small sample masses used in the present experiment lead still to sizable corrections up to ~5%. In the work of Macklin and Winters [7], which was carried out with samples that were up to 14 times heavier, no data are given for this correction. Though much larger corrections are expected in that experiment, their determination was facilitated by the fact that resolved resonances could be fitted at low energies.

The determination of the neutron energy could be checked by means of the ^{126}Te resonances which were resolved at low neutron energies. On average, the agreement with the resonance energies given by Macklin and Winters [7] is better than 100 eV.

IV. RESULTS FOR THE NEUTRON CAPTURE CROSS SECTIONS

The neutron capture cross section ratios of the tellurium isotopes relative to ^{197}Au are listed together with the respective statistical, systematic, and total uncertainties in Table VII. The individual data for the three runs and the two evaluations discussed in Sec. III are given in Ref. [13]. The values of Table VII are weighted averages of the three runs, the weight being determined by the inverse square of the statistical uncertainties. As in our first experiment [10], the results of evaluation 2 were adopted as the final cross section ratios. The uncertainty in the cross section ratio is of the order of 1% and even the small cross section of ^{126}Te could be determined with ~2% accuracy. This is a significant improvement compared to other experimental techniques. The energy binning chosen is fine enough that systematic uncertainties in the calculation of Maxwellian-averaged cross sections (see Sec. VI) are avoided.

The experimental ratios were converted into absolute cross sections by means of the gold cross section of Macklin [23] after normalization by a factor of 0.989 to the absolute value of Ratynski and Käppeler [24]. If these data, given in Table VIII, are used in further work, their uncertainties can be calculated from the uncertainty of the cross section ratio by adding quadratically the 1.5% uncertainty of the standard.

Figure 8 shows a comparison of the present results for the *s*-only isotopes with the data of Macklin and Winters

[7]. On average, the agreement in the energy interval 20 to 100 keV is better than 2.5%, well within the quoted uncertainties. The shape of the ^{125}Te cross section is slightly different. At 100 keV, the present data are lower by ~2% while they are higher by ~4% at 20 keV. An exception is ^{126}Te, where the cross section found in the present experiment is systematically lower by ~15%. In view of this generally good agreement, the comparison to the older data of Bergman and Romanov [25] and Macklin and Gibbons [26] can be taken from Ref. [7].

V. DISCUSSION OF UNCERTAINTIES

The determination of statistical and systematic uncertainties of the present experimental method has been described in Ref. [10]. In the following we consider mainly new aspects that were inherent to the present experiment on the tellurium isotopes. The individual uncertainties are compiled in Table IX.

(i) Background subtraction. The subtraction of the background due to sample scattered neutrons in the odd tellurium isotopes as described in Sec. III may lead to systematic uncertainties in the very low neutron energy range. There, the signal to background ratio is poor and the accuracy of the peak area around 6.9 MeV due to capture in ^{134}Ba and ^{136}Ba is not sufficient for a reliable background subtraction. For this reason, we hesitated to quote the data below 15 keV. The correlated uncertainty in the energy range above 15 keV was estimated to be well below the statistical uncertainty and was therefore neglected. This is confirmed by the fact that for ^{123}Te no systematic deviations from the data of Macklin and Winters [7] are observed at low neutron energies (see Fig. 8). In case of ^{125}Te the situation is not so clear. For this isotope, the shape is slightly different up to 100 keV, which can certainly not be explained by this effect.

(ii) Flight path. The flight path was measured several times during the experiment and was found reproducible

TABLE VII. The final neutron capture cross section ratios of ^{122}Te, ^{123}Te, ^{124}Te, ^{125}Te, and ^{126}Te relative to ^{197}Au together with the statistical and systematic uncertainties in (%) (energy bins as used for the calculation of the Maxwellian-averaged cross sections).

Energy	$\frac{\sigma(^{122}\text{Te})}{\sigma(^{197}\text{Au})}$	Uncertainty			$\frac{\sigma(^{123}\text{Te})}{\sigma(^{197}\text{Au})}$	Uncertainty			$\frac{\sigma(^{124}\text{Te})}{\sigma(^{197}\text{Au})}$	Uncertainty		
(keV)		stat	sys	tot		stat	sys	tot		stat	sys	tot
5–7.5	0.3846	8.0	0.8	8.0					0.1966	11.1	0.8	11.1
7.5–10	0.4461	5.3	0.8	5.4					0.2596	6.4	0.8	6.4
10–12.5	0.4179	3.1	0.8	3.2					0.1969	4.6	0.8	4.7
12.5–15	0.5711	2.3	0.8	2.4					0.2851	2.9	0.8	3.0
15–20	0.5996	1.3	0.8	1.5	1.4292	1.6	0.8	1.8	0.3167	1.6	0.8	1.8
20–25	0.5551	1.1	0.8	1.4	1.5767	1.2	0.8	1.4	0.2977	1.4	0.8	1.6
25–30	0.5239	0.9	0.8	1.2	1.5567	1.0	0.8	1.3	0.2758	1.2	0.8	1.4
30–40	0.5427	0.7	0.8	1.1	1.5575	0.8	0.8	1.1	0.2742	1.0	0.8	1.3
40–50	0.5589	0.7	0.8	1.1	1.6283	0.7	0.8	1.1	0.2772	1.0	0.8	1.3
50–60	0.5072	0.8	0.8	1.1	1.6214	0.8	0.8	1.1	0.2798	1.0	0.8	1.3
60–80	0.5325	0.7	0.8	1.1	1.5739	0.7	0.8	1.1	0.2599	0.9	0.8	1.2
80–100	0.5202	0.8	0.8	1.1	1.5608	0.8	0.8	1.1	0.2755	1.1	0.8	1.4
100–120	0.5136	1.0	0.8	1.3	1.4695	1.1	0.8	1.4	0.2763	1.3	0.8	1.5
120–150	0.5232	0.9	0.8	1.2	1.4706	1.0	0.8	1.3	0.2730	1.2	0.8	1.4
150–175	0.5369	1.0	0.8	1.3	1.4035	1.1	0.8	1.4	0.2904	1.3	0.8	1.5
175–200	0.5621	1.2	0.8	1.4	1.2607	1.3	0.8	1.5	0.2879	1.5	0.8	1.7

Energy	$\frac{(^{125}\text{Te})}{\sigma(^{197}\text{Au})}$	Uncertainty			$\frac{\sigma(^{126}\text{Te})}{\sigma(^{197}\text{Au})}$	Uncertainty		
(keV)		stat	sys	tot		stat	sys	tot
5–7.5					0.1210	17.1	1.0	17.1
7.5–10					0.1218	13.2	1.0	13.2
10–12.5					0.1603	5.3	1.0	5.4
12.5–15					0.1531	5.0	1.0	5.1
15–20	0.8850	1.4	0.8	1.6	0.2174	2.4	1.0	2.6
20–25	1.0192	1.1	0.8	1.4	0.1522	2.6	1.0	2.8
25–30	0.9338	0.9	0.8	1.2	0.1448	2.2	1.0	2.4
30–40	0.8681	0.7	0.8	1.1	0.1356	1.8	1.0	2.1
40–50	0.8673	0.7	0.8	1.1	0.1412	1.8	1.0	2.1
50–60	0.7440	0.7	0.8	1.1	0.1500	1.8	1.0	2.1
60–80	0.6467	0.7	0.8	1.1	0.1321	1.7	1.0	2.0
80–100	0.6077	0.9	0.8	1.2	0.1362	2.0	1.0	2.2
100–120	0.5312	1.1	0.8	1.4	0.1385	2.4	1.0	2.6
120–150	0.5009	1.0	0.8	1.3	0.1395	2.3	1.0	2.5
150–175	0.4707	1.2	0.8	1.4	0.1405	2.4	1.0	2.6
175–200	0.4687	1.4	0.8	1.6	0.1455	2.6	1.0	2.8

TABLE VIII. The neutron capture cross section of ^{122}Te, ^{123}Te, ^{124}Te, ^{125}Te, and ^{126}Te calculated from the experimental ratios using the gold data from literature [23,24].

Energy (keV)	$\sigma(^{197}Au)$ (mb)	$\sigma(^{122}Te)$ (mb)	$\sigma(^{123}Te)$ (mb)	$\sigma(^{124}Te)$ (mb)	$\sigma(^{125}Te)$ (mb)	$\sigma(^{126}Te)$ (mb)
5–7.5	1726.7	664.1		339.5		209.0
7.5–10	1215.7	542.3		315.6		148.1
10–12.5	1066.7	445.8		210.1		171.0
12.5–15	878.0	501.4		250.4		134.4
15–20	738.8	443.0	1055.9	234.0	653.8	160.6
20–25	600.0	333.1	946.1	178.6	611.5	91.3
25–30	570.8	299.0	888.6	157.5	533.1	82.7
30–40	500.4	271.6	779.4	137.2	434.4	67.9
40–50	433.3	242.2	705.6	120.1	375.8	61.2
50–60	389.6	197.6	631.7	109.0	289.9	58.5
60–80	349.4	186.1	549.9	90.8	226.0	46.2
80–100	298.3	155.2	465.6	82.2	181.3	40.6
100–120	290.1	149.0	426.3	80.2	154.1	40.2
120–150	274.1	143.4	403.2	74.8	137.3	38.2
150–175	263.7	141.5	370.0	76.6	124.1	37.1
175–200	252.6	142.0	318.4	72.7	118.4	36.8

within an accuracy of ±0.1 mm. In spite of the fact that the thickness of the samples varied between 0.8 and 5 mm, the mean flight path of the samples agreed within ±0.1 mm. Therefore, the uncertainty of 0.1% quoted in Ref. [10] was found to be a reasonable estimate for the present experiment, too.

(iii) Sample mass. The uncertainty in the sample mass is dominated by the accuracy of the oxygen content, which is ±0.04% in case of samples with low contamination (see Table II) and ±0.1% for ^{123}Te. These results were confirmed in repeated measurements, and are, therefore, representative for the powder material. The final samples were prepared and weighed at the same time when the oxygen content was determined to made sure that no changes in stoichiometry took place. Actually, the weight of the samples increased in the time between preparation and canning by 0.2 mg in spite of the fact that they were always kept in an argon atmosphere. After canning in a thin polyethylene foil, the weight increased during the seven months of the measurement by 0.6–1.7 mg/sample corresponding to less than 0.1% of the weight. Again, the situation was different for the ^{123}Te sample that showed an increase of 3%. The additional mass is supposed to be due to further absorption of oxygen. While this does not affect the uncertainty of the mass determination, it increased the uncertainty of the multiple scattering correction (see below).

Impurities by other elements in the sample material were analyzed by the suppliers and found to be below the detection limits between 0.05% and 0.005%. It is not expected that these impurities can affect the sample mass beyond the uncertainty of 0.1% given in Table IX.

(iv) Isotopic enrichment. In the measurement of the isotopic composition performed at KfK, abundances of 5% could be determined with an uncertainty of ≤1% and abundances of 0.5% with an uncertainty of ≤3%. From these values, an uncertainty of 2% can be interpo-

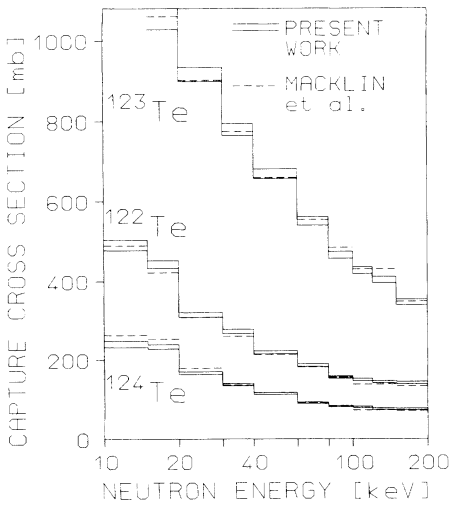

FIG. 8. The neutron capture cross section of the *s*-only tellurium isotopes in the energy range from 10 to 200 keV (open bars) in comparison with the data of Macklin and Winters [7].

TABLE IX. Systematic uncertainties (%).

Flight path (cross section ratio)		0.1
Neutron flux normalization (cross section ratio)		0.2
Sample mass (tellurium isotopes)		0.1
Isotopic enrichment (tellurium isotopes)		0.2
Multiple scattering	(Au)	0.3
	(^{122}Te)	0.3
	(^{123}Te)	0.2
	(^{124}Te)	0.3
	(^{125}Te)	0.3
	(^{126}Te)	0.7
Unobserved events (cross section ratio)		0.6
Total	$\sigma(^{122}Te)/\sigma(Au)$	0.8
systematic	$\sigma(^{123}Te)/\sigma(Au)$	0.8
uncertainties	$\sigma(^{124}Te)/\sigma(Au)$	0.8
	$\sigma(^{125}Te)/\sigma(Au)$	0.8
	$\sigma(^{126}Te)/\sigma(Au)$	1.0

lated for a typical isotopic impurity of 2% (Table III). Since the samples are enriched to 90% or more, the 10% impurities were determined with an average uncertainty of 2%. This leads to an uncertainty of 0.2% for the main isotope which was taken as the systematic uncertainty. This is a reasonable estimate according to the differences between our results and those of the suppliers.

The only remarkable discrepancy is the ^{123}Te content of the ^{122}Te sample, where a difference of 0.6% was found. The sum of the isotopes 122 and 123, however, agrees to better than 0.1%. This leads to the idea that a limited mass resolution prevented a complete separation of the weak intensity of isotope 123 from the strong 122 component in one of the measurements. The mass separators used at KfK have a mass resolution of 500. It implies that for a mass around 100 the full width at tenth of the maximum of a peak in the mass spectrum is a factor of five smaller than the distance to the next isotope. Thus an incomplete mass separation can be excluded in our analysis and our data were assumed to be correct.

(v) Isotopic correction. The uncertainty discussed above causes an uncertainty in the number of atoms in the sample $m(X)$ [see Eq. (1)]. An additional uncertainty comes from the fact that part of the count rate Z_i is removed to account for the other isotopes as described in Sec. III. Fortunately, in the present experiment this correction is small. For the even isotopes it is dominated by the impurities of odd isotopes as they have larger cross sections. But as they have higher binding energies, too, the spectrum is changed essentially in the sum energy region around 9 MeV that is not used for the evaluation of the even isotopes at all. On the other hand, the correction for the odd isotopes is small since the even isotopes, which dominate the impurities, have significantly smaller cross sections. In the TOF spectra (see, e.g., Fig. 4) used for the determination of the cross section shape, the reduction in count rate by the isotopic correction was only 1–2 % with maximum values of ~4% for the ^{124}Te sample. This correction is known with a systematic uncertainty of 2%, yielding a negligible uncertainty of less than 0.1%.

The corrections *(iv)* and *(v)* partly compensate for each other, the combined effect being smaller than if they are treated independently. Thus even the 0.6% discrepancy in the ^{123}Te content of the ^{122}Te sample would not change the final cross section by more than 0.4%.

(vi) Dead time and pileup. Systematic uncertainties correlated with these effects were discussed in Ref. [10] and were found to be negligible.

(vii) Normalization to equal neutron flux. In the present experiment only the count rate of the neutron monitor close to the neutron target was used for normalization. Therefore, we slightly increased the corresponding uncertainty for the cross section ratio to 0.2%. This seems rather conservative since the corrections themselves are smaller than 1% (see Ref. [13]).

(viii) Spectrum fraction. The systematic uncertainty of the fraction of unobserved capture events F_1 [see Eq. (1)] was discussed in detail in Ref. [10], where a systematic uncertainty of 0.6% was found. This discussion is still valid for the present experiment but part of the uncertainties are not relevant for the tellurium isotopes and affect only the gold spectrum. All cascades up to multiplicity 6 were included in the calculations. The variation of the energy threshold between 0 and 100 keV is irrelevant for capture in ^{122,123,125}Te since no transitions below 100 keV are observed in the compound nucleus. Thus the quoted uncertainty of 0.6% is still acceptable for the cross section ratio of the tellurium isotopes relative to the gold standard. In our *s*-process studies (see Sec. VII), where only the cross section ratios $\sigma(^{122}\text{Te})/\sigma(^{124}\text{Te})$ and $\sigma(^{123}\text{Te})/\sigma(^{124}\text{Te})$ are important, the uncertainty in the cross section ratio is even smaller because the uncertainty due to the gold spectrum cancels out.

The calculation of the fraction of unobserved capture events was checked by evaluating the run with 100 keV maximum neutron energy for a threshold in the sum energy of 1.9 and 2.4 MeV. This difference affects only the normalization factor

$$N=\sum Z(\text{Au})\sum E(X)\Big/\sum Z(X)\sum E(\text{Au}) \tag{2}$$

and F_1 [see Eq. (1)], but their product should remain unchanged. The respective values are given in Ref. [13]. Both evaluations differ on average by ~1%, but this difference can fully be explained by the statistical uncertainty of N and the systematic uncertainty of F_1. A larger systematic uncertainty in F_1 should show up immediately for the odd isotopes for which the correction is a factor of ten larger than for the even isotopes. In our final results given in Table VII the higher threshold was used in this run, too, since the statistical uncertainty is smaller for that choice.

(ix) Multiple scattering. The multiple scattering and self-shielding correction was calculated with different input parameters to study the systematic uncertainties. It turned out that this correction is most sensitive to the total cross section. For the odd isotopes the size of the correction is generally small because of the small sample mass and because multiple scattering (MS) and self-shielding compensate each other. The effect of the total cross section is much larger for the even isotopes. Especially the small capture cross section of ^{126}Te and the large sample mass had the consequence that MS is strongly dependent on the total cross section. The uncertainties given in Table IX were derived from the assumption that the total cross section was reproduced within ±5% in the calculation.

The oxygen content had to be considered in the systematic uncertainty, too. The calculations for the ^{123}Te sample showed that a contamination of 12% changes the correction by 0.008 on average. This result was used to estimate the systematic uncertainties caused by neglecting the initial oxygen content of all samples except for ^{123}Te and by the increase in mass observed during the experiment.

These estimates of the systematic uncertainties are correct for most of the energy range covered, but it seems somewhat optimistic for the values derived for ^{124}Te and ^{126}Te at 10 keV. The assumption on the total cross sections of ^{125,126}Te that were mainly based on the systemat-

TABLE X. Maxwellian-averaged neutron capture cross sections of the tellurium isotopes 122 to 126. The uncertainty of 1.5% of the gold standard is not included in the quoted uncertainty since it cancels out in most applications of relevance for nuclear astrophysics (see Sec. VII).

kT (keV)	^{122}Te (mb)	^{123}Te (mb)	^{124}Te (mb)	^{125}Te (mb)	^{126}Te (mb)
10	541.1±6.2	1436.1±16.6	288.8±3.5	815.2±10.9	152.1±2.9
12	488.7±5.2	1310.3±14.0	259.9±3.0	745.0±8.8	138.0±2.6
20	367.9±3.6	1017.2±9.8	194.6±2.1	560.4±5.5	103.0±1.8
25	325.6±3.1	910.8±8.5	171.0±1.8	486.8±4.7	90.3±1.5
30	295.4±2.7	831.5±7.7	154.6±1.6	431.2±4.0	81.3±1.4
40	255.2±2.3	718.9±6.6	133.3±1.4	353.4±3.3	69.5±1.1
50	230.3±2.1	641.2±5.9	120.4±1.3	302.2±2.8	62.2±1.0
52	226.4±2.1	628.2±5.8	118.2±1.1	294.1±2.6	61.0±1.0
60	213.6±1.9	583.4±5.4	111.5±1.1	266.6±2.4	57.3±0.9
70	201.8±1.9	538.3±4.9	105.6±1.0	240.5±2.2	53.9±0.9
80	193.1±1.7	501.7±4.6	101.0±1.0	220.6±2.1	51.4±0.8
90	186.0±1.7	470.9±4.3	97.5±0.9	204.6±1.8	49.4±0.7
100	180.2±1.6	444.3±4.1	94.5±1.0	191.4±1.7	47.7±0.7

ics of the other isotopes may also be criticized. But with the detailed information given in Ref. [13] it should be possible to derive revised values for this correction if new data for the total cross sections become available that differ significantly from the adopted ones.

VI. MAXWELLIAN-AVERAGED CROSS SECTIONS

The Maxwellian-averaged cross sections were calculated in the same way as described in Refs. [10] and [27]. The neutron energy range from 0 to 600 keV was divided into four parts I_1 to I_4, according to the cross sections from different sources. The contribution I_1 at low neutron energies is calculated from resonance parameters, while I_3 covers the range of the present experiment. In parts I_2 and I_4 above and below, respectively, the cross section shape was taken from literature and normalized to the present data. The individual contributions are tabulated in Ref. [13]. The values I_3 were calculated using the cross sections in the energy binning given in Table VIII, which is fine enough to make the correlated systematic uncertainty negligible. For the three s-only isotopes ^{122,123,124}Te, I_1 had to be calculated from resonance parameters [20] only in the interval from 0 to 1 keV. For part I_2 we used the data of Xia *et al.* [22] that were normalized to the present data in the overlapping energy range. This procedure was applicable since the cross section shapes were practically identical. The energy interval from 200 to 600 keV that contributes only very little to the Maxwellian average at typical s-process temperatures was covered by the data of Macklin and Winters [7] normalized in the same way. For the isotopes ^{125,126}Te the data of Ref. [7] had to be used in the low energy range, too, and I_1 was extended from 0 to 3 keV. The uncertainties of the individual parts, δI_x, are discussed in Ref. [13].

The systematic uncertainty of the Maxwellian-averaged cross section is the uncertainty of the cross section ratio (see Table VII) which has to be assigned to the summed intensity $I_2+I_3+I_4$. The 1.5% uncertainty of the gold standard was not included since it cancels out in most applications of relevance for s-process studies (see Sec. VII). The Maxwellian-averaged cross sections together with their total uncertainty are given in Table X. For temperatures in excess of $kT=20$ keV it is dominated by the systematic uncertainty.

We note that in determining ratios, as, e.g., $\langle\sigma\rangle(^{122}\text{Te})/\langle\sigma\rangle(^{124}\text{Te})$, it is not allowed to add the uncertainties given in Table VII quadratically, because they are highly correlated. For example, the statistical uncertainties of the cross section ratios are partly determined by the count rate in the gold spectra $[Z_i(\text{Au}), \sum Z(\text{Au}), \sum E(\text{Au})$ in Eq. (1)], which cancels out in the cross section ratio of two tellurium isotopes. The same holds for the systematic uncertainties for multiple scattering and for the spectrum fraction of the gold sample. The exact uncertainty of the ratio of Maxwellian-averaged cross sections of two tellurium isotopes is complicated to determine and will be discussed in detail in Sec. VII. As an estimate, the larger value of the two cross sections involved in the ratio could be used, since statistical and systematic uncertainties of the gold sample

TABLE XI. Input data for the stellar neutron capture cross sections used in the calculations according to the classical model.

Isotope	$\langle\sigma\rangle$ (mb)[a]	Reference
^{116}Sn	93.6±5	Beer *et al.* [34]
^{117}Sn	409±78	Bao and Käppeler [14]
^{118}Sn	64±12	Bao and Käppeler
^{119}Sn	251±48	Bao and Käppeler
^{120}Sn	32.5±1.4	Schanz [33]
^{121}Sn^m	194	Holmes *et al.* [35]
^{122}Sn	23±5	Bao and Käppeler
^{121}Sb	541±15	Schanz
^{123}Sb	309±9	Schanz
^{122}Te	300.5±2.7	Present work
^{123}Te	845.7±7.8	Present work
^{124}Te	157.2±1.6	Present work

[a]Maxwellian-averaged cross sections at $kT=29$ keV, extrapolated according to $1/v$ from the data given for $kT=30$ keV.

TABLE XII. *s*-process production ratios of ^{122}Te, ^{123}Te, and ^{124}Te relative to solar abundances (normalized at ^{124}Te).

	Classical model		Low mass stars	
Isotope	Present work	Macklin[a]	Present work	Macklin[a]
^{122}Te	0.984±0.012	1.032±0.057	0.91±0.01[b]	0.96±0.06[b]
^{123}Te	1.003±0.012	1.021±0.051	0.94±0.01[b]	0.96±0.05[b]
^{124}Te	1	1	1	1

[a]Capture cross sections from Macklin and Winters [7].
[b]Error bars due to uncertainty of the capture cross section of tellurium isotopes. An additional uncertainty of ~0.01 comes from the cross sections of the unstable isotopes ^{121}Sn and ^{122}Sb.

and the tellurium samples are similar.

If we compare the present results with the data of Macklin and Winters [7] for $kT=20-30$ keV, good agreement is found for the isotopes ^{123,124,125}Te. A little bit surprising is the result for ^{122}Te, where a 6% difference is obtained which is not expected from the good agreement of both data sets in the neutron energy range from 20 to 100 keV. At $kT=10$ keV even larger discrepancies are found. The largest differences are observed for ^{126}Te.

VII. IMPLICATIONS FOR THE CLASSICAL *s*-PROCESS AND FOR STELLAR MODELS

The classical concept of the *s* process dates back to the basic paper by Burbidge *et al.* [28] and simply assumes the irradiation of a certain fraction G of the observed ^{56}Fe abundance by a suited neutron exposure. This approach has been detailed by Seeger, Fowler, and Clayton [29], who showed that the observed *s*-process abundances can be described by means of an exponential distribution of neutron exposures τ,

$$\rho(\tau)=\frac{GN_{\odot}^{56}}{\tau_0}\exp(-\tau/\tau_0)\ , \tag{3}$$

τ being the time integrated neutron flux.

This assumption on the type of neutron exposure is characterized by only two parameters, the fraction G of the observed ^{56}Fe abundance and the mean neutron exposure, τ_0; it allows one to solve analytically the set of coupled differential equations describing the abundances of the entire neutron capture chain from iron to bismuth. However, this solution requires two simplifications, i.e., that the neutron density and the temperature are constant throughout the duration of the *s* processes. Then, the characteristic quantity describing the *s*-process flow, the product $\langle\sigma\rangle N_s$ of the stellar cross section, $\langle\sigma\rangle$, and the *s*-process abundance, N_s, can be expressed as a function of mass number [30]:

$$\langle\sigma\rangle N_s(A)=\frac{GN_{\odot}^{56}}{\tau_0}\prod_{i=56}^{A}\left[1+\frac{1}{\langle\sigma\rangle_i\tau_0}\right]^{-1}\ , \tag{4}$$

which depends only on the Maxwellian-averaged neutron capture cross sections, $\langle\sigma\rangle_i$, along the neutron capture chain. The two parameters, G and τ_0, are determined by a least-squares fit of the $\langle\sigma\rangle N_s(A)$ curve to the empirical $\langle\sigma\rangle N_s$ values of those nuclei, which are produced exclusively by the *s* process. A detailed description of the classical *s*-process approach is given in Refs. [1] and [31].

In deriving Eq. (4), it was additionally assumed that the neutron capture rates should be either much faster or much slower than the beta decay rates of the unstable isotopes produced. In other words, possible branchings of the neutron capture path due to competition between beta decays and neutron captures were neglected. The proper treatment of branchings in the framework of the classical approach was formulated by Ward, Newman, and Clayton [32] and is given in Ref. [31]. The strength of a branching can be described by the branching factor f_n or f_β (see Sec. I). In the following we use the factor $f_\beta=\lambda_\beta/(\lambda_\beta+\lambda_n)$ instead of f_n in order to keep the formulas simpler.

The *s*-process path in the region of the tellurium isotopes is shown in Fig. 1. There are two possible branching points at the unstable isotopes ^{121}Sn and ^{122}Sb. The situation is complicated by the fact that neutron capture in ^{120}Sn may lead either to the ground state or the isomeric state in ^{121}Sn, that have to be treated independently [33]. The fraction of capture events to the isomer is defined as IR. In case of neutron capture in ^{121}Sb there is an isomeric state, too, but as both ground state and isomer have about the same half-life they can be treated as a single isotope. For this branching, however, one has to consider the possibility of β^+ decay or electron capture (EC) to ^{122}Sn, giving rise to the branching factors $f_{\mathrm{EC},\beta^+}=\lambda_{\mathrm{EC},\beta^+}/(\lambda_{\beta^-}+\lambda_{\mathrm{EC},\beta^+}+\lambda_n)$ and $f_{\beta^-}=\lambda_{\beta^-}/(\lambda_{\beta^-}+\lambda_{\mathrm{EC},\beta^+}+\lambda_n)$. In this relation λ_{EC} and λ_{β^+} are the decay rates for the respective decays defined in the same way as the decay rate for β^- decay (see Sec. I).

Equation (4) can also be written as a recursive formula:

$$\langle\sigma\rangle N(^AZ)=\zeta(^AZ)\langle\sigma\rangle N(^{A-1}Z)\ , \tag{5a}$$

with the propagator

$$\zeta(^AZ)=\left[1+\frac{1}{\tau_0\langle\sigma\rangle(^AZ)}\right]^{-1}\ . \tag{5b}$$

If ^AZ is a branch point, the propagator ζ has to be replaced by

$$\xi(^{A}Z)=\left[\frac{1}{1-f_{\beta}}+\frac{1}{\tau_0\langle\sigma\rangle(^{A}Z)}\right]^{-1}, \quad (6)$$

to calculate the $\langle\sigma\rangle N$ value in the neutron-rich part of the branching. The contribution to the isobar $Z+1$ via β^- decay is then given by

$$\langle\sigma\rangle N(^{A}(Z+1))=\frac{f_{\beta}}{1-f_{\beta}}\xi(^{A}(Z+1))\langle\sigma\rangle N(^{A}Z) . \quad (7)$$

The s-process path from ^{119}Sn to ^{124}Te is described by the following equations [33]:

$$\langle\sigma\rangle N(^{120}\text{Sn})=\xi(^{120}\text{Sn})\langle\sigma\rangle N(^{119}\text{Sn}) , \quad (8)$$

$$\langle\sigma\rangle N(^{121}(\text{Sn}^m)=IR\,\xi(^{121}\text{Sn}^m)\langle\sigma\rangle N(^{120}\text{Sn}) , \quad (9)$$

$$\langle\sigma\rangle N(^{122}\text{Sn})=\xi(^{122}\text{Sn})\left[\langle\sigma\rangle N(^{121}\text{Sn}^m)+\frac{f_{EC,\beta^+}(^{122}\text{Sb})}{1-f_{\beta^-}(^{122}\text{Sb})-f_{\text{EC},\beta^+}(^{122}\text{Sb})}\langle\sigma\rangle N(^{122}\text{Sb})\right] , \quad (10)$$

$$\langle\sigma\rangle N(^{121}\text{Sb})=\xi(^{121}\text{Sb})\left[(1-IR)\langle\sigma\rangle N(^{120}\text{Sn})+\frac{f_{\beta}(^{121}\text{Sn}^m)}{1-f_{\beta}(^{121}\text{Sn}^m)}\langle\sigma\rangle N(^{121}\text{Sn}^m)\right] , \quad (11)$$

$$\langle\sigma\rangle N(^{122}\text{Sb})=\xi(^{122}\text{Sb})\langle\sigma\rangle N(^{121}\text{Sb}) , \quad (12)$$

$$\langle\sigma\rangle N(^{123}\text{Sb})=\xi(^{123}\text{Sb})[\langle\sigma\rangle N(^{122}\text{Sn})+\langle\sigma\rangle N(^{122}\text{Sb})] , \quad (13)$$

$$\langle\sigma\rangle N(^{122}\text{Te})=\xi(^{122}\text{Te})\frac{f_{\beta^-}(^{122}\text{Sb})}{1-f_{\beta^-}(^{122}\text{Sb})-f_{\text{EC},\beta^+}(^{122}\text{Sb})}\langle\sigma\rangle N(^{122}\text{Sb}) , \quad (14)$$

$$\langle\sigma\rangle N(^{123}\text{Te})=\xi(^{123}\text{Te})\langle\sigma\rangle N(^{122}\text{ Te}) , \quad (15)$$

$$\langle\sigma\rangle N(^{124}\text{Te})=\xi(^{124}\text{Te})[\langle\sigma\rangle N(^{123}\text{Te})+\langle\sigma\rangle N(^{123}\text{Sb})] . \quad (16)$$

This set of equations was solved to determine the s-process abundances of the isotopes ^{122,123,124}Te which can then be compared to the abundances observed in the solar system. For this purpose a variety of input parameters are necessary.

Neutron capture cross sections. The neutron capture cross sections for the s-only isotopes were taken from the present investigation. Three of the other involved isotopes have recently been measured at KfK using the activation technique [33], the others were taken from literature [14,34,35]. The actual values are compiled in Table XI.

Neutron density and temperature. The parameters that are required to calculate λ_n and λ_β were adopted from an evaluation of all important branchings [31]:

$$n_n=(3.4\pm1.1)\times10^8\ \text{cm}^{-3} ,$$

$$kT=29\pm5\ \text{keV},\quad T=(3.3\pm0.5)\times10^8\ \text{K} .$$

Mean neutron irradiation. The isotopes under investigation are completely formed by the main component of the s-process flow, which is characterized by a mean neutron exposure [31]:

$$\tau_0=0.295\pm0.009\ \text{mb}^{-1} .$$

Beta-decay rates. The beta-decay rates of unstable isotopes may be drastically changed under stellar conditions. In the present investigation such an enhancement can be expected for the beta decay of ^{121}Sn. According to the calculations of Takahashi and Yokoi [36] the decay rate is increased by a factor 2.9 at a temperature of 3.3×10^8 K. This enhancement, however, is valid only for a thermal equilibrium between ground state and isomer. As discussed in Ref. [33], which followed the procedure recommended by Klay *et al.* [37], thermal equilibrium is not reached in ^{121}Sn. This means that the isomeric state is slowly depopulated to the ground state, resulting in a situation of approximate decoupling between these states.

With the parameters compiled above, the abundances N_s of the s-only isotopes ^{122,123,124}Te were calculated and the ratio to the solar abundances, $N_s/N_\odot$, was determined. The results were normalized to unity at ^{124}Te since this isotope experiences the entire mass flow. This procedure allows us to use the isotopic abundances given with an accuracy of about 0.1% in Ref. [6] [^{122}Te 2.603 (3), ^{123}Te 0.908 (1), and ^{124}Te 4.816 (3)]. The results are compiled in Table XII. For a perfect model, all values should be unity. Obviously, the classical approach comes very close to this ideal case. For the first time, the prediction of the classical model of the "local approximation," i.e., that the product $\langle\sigma\rangle N_s$ is constant for neighboring isotopes, could be checked on the 1% level for a set of three s-only isotopes. The neutron density of the classical model is sufficiently low that the branchings at ^{121}Sn and ^{122}Sb remain inefficient. Within the experimental uncertainties, a very weak branching of at most ~1% would be possible if one considers the $\langle\sigma\rangle N_s$ values of

^{123}Te and ^{124}Te only (for ^{122}Te see below), corresponding to an upper limit for the neutron density of

$$n_n < 6.0 \times 10^8 \text{ cm}^{-3} .$$

The uncertainty of the predicted *s*-process abundances is completely dominated by the uncertainty of the ratios:

$$\langle \sigma \rangle N_s(^{122}\text{Te}) / \langle \sigma \rangle N_s(^{124}\text{Te})$$

and

$$\langle \sigma \rangle N_s(^{123}\text{Te}) / \langle \sigma \rangle N_s(^{124}\text{Te}) .$$

The abundances being known with a negligible uncertainty of 0.1% implies further that the uncertainty is determined by the cross section ratio only. This uncertainty cannot be calculated from the values given in Table X (see Sec. VI) since the uncertainties related to the gold sample cancel out in the ratio. Therefore, a thorough correlation analysis was performed yielding the uncertainties for the Maxwellian-averaged cross section ratios that are given in Ref. [13]. An uncertainty of $\sim 1.2\%$ was evaluated for the cross section ratios $\langle \sigma \rangle (^{122}\text{Te}) / \langle \sigma \rangle (^{124}\text{Te})$ and $\langle \sigma \rangle (^{123}\text{Te}) / \langle \sigma \rangle (^{124}\text{Te})$.

The present results for the classical model allow also for a discussion of limits for the *p*-process abundances of the tellurium isotopes. There is agreement among current *p*-process models [38,39] that the odd isotope ^{123}Te is not produced in the high temperature regime of the *p*-process. In this case, the equality of the $\langle \sigma \rangle N_s$ values of ^{123}Te and ^{124}Te has the consequence that the *p*-process contribution to ^{124}Te is also zero. Therefore, it is not possible that a weak branching may be compensated by *p*-process contributions to ^{122}Te and ^{123}Te. It has to be noted that the tellurium isotopes provide for the only branching with three *s*-only nuclei including an odd isotope where such a test is possible. Hence, the abundance ratio of 0.984 derived for ^{122}Te could be interpreted as a 1.5% *p*-process contribution. Given the experimental uncertainties, this is not a quantitative assignment, but it appears quite reasonable if it is compared to the abundance of the pure *p* nucleus ^{120}Te, which is $\sim 3\%$ of the ^{122}Te abundance.

The cross sections obtained in the present experiment were also used to calculate the *s*-process abundances in the Te region with a stellar model. At present, the most successful approach is the stellar helium burning in low mass stars (Gallino *et al.* [31,40]), that allows for a quantitative description of the abundance pattern of the main component. Adopting the profiles for neutron density, temperature, and mass density from this model [41], the *s*-process flow through the mass region $110 < A < 130$ was followed with the network code NETZ [42]. Preliminary results are included in Table XII, indicating that this model predicts significant branchings at $A = 121, 122$, which cause $\sim 6\%$ of the flow to bypass ^{122}Te and ^{123}Te. This is mostly due to the higher neutron density implied by the stellar model compared to the classical approach. A detailed discussion of this discrepancy and its astrophysical implications will be presented in a forthcoming publication [43].

The importance of using very accurate cross sections in these investigations is underlined, if the above *s*-process studies are repeated using respective data of Macklin and Winters [7]. In this case, the significant difference between the classical approach and the stellar model is completely masked by the larger uncertainties of $\sim 5\%$. Obviously, the new experimental technique allows for a much more detailed discussion of the information contained in the observed abundances, and, hence, represents a significant step towards a deeper understanding of the *s* process and of the helium burning stages in stellar evolution.

VIII. CONCLUSIONS

A new experimental setup was used to determine the neutron capture cross sections of the tellurium isotopes in the energy range from 10 to 200 keV. The essential features of this experiment are high efficiency and good energy resolution for the detection of capture gamma rays as well as good time resolution and low sensitivity to sample scattered neutrons. Furthermore, the short primary flight path could be used to discriminate the background due to capture of sample scattered neutrons in the detector via time of flight. This unique combination allowed us to determine the cross section ratio of the tellurium isotopes to the gold standard with an uncertainty of $\sim 1\%$, which represents an improvement of a factor of five compared to conventional techniques.

Accurate cross sections are essential for detailed studies of the element production in the *s* process. For obtaining the stellar cross sections, the measured energy range was extended to thermal and to 600 keV by normalizing the cross section shape from literature to the present results. In this way, it was possible to determine the stellar values for astrophysical applications with $\sim 1\%$ uncertainty, too.

With these data it could be shown for the first time that the classical *s*-process model describes the solar abundances of *s*-only nuclei at least locally very well, i.e., that the "local approximation" ($\langle \sigma \rangle N_s = \text{const}$ for neighboring isotopes) is valid with an uncertainty of 1%. It was also possible to derive limits for the *p*-process contributions of the *s*-only isotopes of tellurium. Preliminary calculations with a stellar model confirmed that the accurate data are essential for deciphering the information in the observed abundances, and to derive true constraints for the stellar environment.

The present experiment begins a series of measurements for a systematic investigation of those branchings in the *s*-process path that are characterized by two *s*-only nuclei, with the next examples being the pairs ^{148}Sm/^{150}Sm, ^{134}Bd/^{136}Ba, ^{128}Xe/^{130}Xe, and ^{152}Gd/^{154}Gd. These results will allow us to analyze known branchings with improved accuracy and to check for possible weak branchings presently presumed by model predictions. In this way, the $\langle \sigma \rangle N_s$ curve can be defined very accurately, and rather stringent predictions may be expected for the physical conditions during the *s* process. These investigations, complemented by other new experiments, e.g., cross section studies for the radioactive branch point isotopes, will allow us to use the *s* process as a diagnostic

tool for the stellar plasma, yielding improved insight in the mechanisms of helium shell burning in red giants.

ACKNOWLEDGMENTS

Many colleagues from KfK helped us to bring this experiment to a successful end. In particular we would like to thank Ch. Adelhelm, E. Nold, and G. Streib from the Institute of Material Research for their careful analyses of the oxygen and hydrogen content of the sample material. We also appreciated the spontaneous help of E. Gantner, H. Deutsch, and J. Reinhardt from the Institute of Radiochemistry who determined the isotopic composition. The Van de Graaff crew, D. Roller, E.-P. Knaetsch, and W. Seith, did a great job in keeping the accelerator running at optimum conditions. Last but not least, the continuous support of G. Rupp in optimizing the experimental setup is gratefully acknowledged.

[1] F. Käppeler, H. Beer, and K. Wisshak, Rep. Prog. Phys. **52**, 945 (1989).
[2] E. Anders and N. Grevesse, Geochim. Cosmochim. Acta **53**, 197 (1989).
[3] H. Holweger, in *Les Elements et leurs Isotopes dans l'Univers,* edited by A. Boury, N. Grevesse, and L. Remy-Battian (University of Liège, Liège, 1979), p. 117.
[4] P. J. Patchett, 46th Annual Meeting of the Meteoritical Society, Mainz, Federal Republic of Germany, 1983 (unpublished).
[5] H. Beer, G. Walter, R. L. Macklin, and P. J. Patchett, Phys. Rev. C **30**, 464 (1984).
[6] N. E. Holden, R. L. Martin, and I. L. Barnes, Pure Appl. Chem. **56**, 675 (1984).
[7] R. L. Macklin and R. R. Winters, Oak Ridge National Laboratory Report ORNL-6561, 1989.
[8] R. R. Winters, F. Käppeler, K. Wisshak, A. Mengoni, and G. Reffo, Astrophys. J. **300**, 41 (1986).
[9] K. Wisshak, K. Guber, F. Käppeler, J. Krisch, H. Müller, G. Rupp, and F. Voss, Nucl. Instrum. Methods **A292**, 595 (1990).
[10] K. Wisshak, F. Voss, F. Käppeler, and G. Reffo, Phys. Rev. C **42**, 1731 (1990).
[11] G. Winkler, Nucl. Instrum. Methods **A282**, 317 (1989).
[12] M. Mizumoto and M. Sugimoto, Nucl. Instrum. Methods **A282**, 324 (1989).
[13] K. Wisshak, F. Voss, F. Käppeler, and G. Reffo, Kernforschungszentrum Karlsruhe Report KfK 4899, 1991.
[14] Z. Y. Bao and F. Käppeler, At. Data Nucl. Data Tables **36**, 411 (1987).
[15] G. Reffo, F. Fabbri, K. Wisshak, and F. Käppeler, Nucl. Sci. Eng. **80**, 630 (1982).
[16] K. Wisshak, F. Käppeler, and G. Schatz, Nucl. Instrum. Methods **221**, 385 (1984).
[17] F. H. Fröhner, SESH—A Fortran IV Code for Calculating the Self-Shielding and Multiple Scattering Effects for Neutron Cross Section Data Interpretation in the Unresolved Resonance Region, Gulf General Atomic Report GA-8380, 1968.
[18] A. Gilbert and A. G. W. Cameron, Can. J. Phys. **43**, 1446 (1965).
[19] R. M. Musaelyan and V. M. Skorkin, Bull. Acad. Sci. USSR **52**, 157 (1988).
[20] S. F. Mughabghab, M. Divadeenam, and N. E. Holden, *Neutron Cross Sections* (Academic, New York, 1981), Vol. 1, Part A.
[21] C. Nordborg, H. Gruppelaar, and M. Salvatores, Proceedings of the International Conference on Nuclear Data for Science and Technology, Jülich, Germany, 1991 (unpublished).
[22] Y. Xia, Th. W. Gerstenhöfer, S. Jaag, F. Käppeler, and K. Wisshak, Phys. Rev. C **45**, 2487 (1992), the following paper.
[23] R. L. Macklin, private communication (1982).
[24] W. Ratysnki and F. Käppeler, Phys. Rev. C **37**, 595 (1988).
[25] A. A. Bergman and S. A. Romanov, Yad. Fiz. **20**, 252 (1975) [Sov. J. Nucl. Phys. **20**, 133 (1975)].
[26] R. L. Macklin and J. H. Gibbons, Phys. Rev. **159**, 1007 (1967).
[27] H. Beer, F. Voss, and R. R. Winters, Astrophys. J. Suppl. **79** (1992).
[28] E. M. Burbidge, G. R. Burbidge, W. A. Fowler, and F. Hoyle, Rev. Mod. Phys. **29**, 547 (1957).
[29] P. A. Seeger, W. A. Fowler, and D. D. Clayton, Astrophys. J. Suppl. **11**, 121 (1965).
[30] D. D. Clayton and R. A. Ward, Astrophys. J. **193**, 397 (1974).
[31] F. Käppeler, R. Gallino, M. Busso, G. Picchio, and C. M. Raiteri, Astrophys. J. **354**, 630 (1990).
[32] R. A. Ward, M. J. Newmann, and D. D. Clayton, Astrophys. J. Suppl. **31**, 33 (1976).
[33] W. Schanz, Diploma thesis, University of Karlsruhe, 1990 (unpublished).
[34] H. Beer, G. Walter, and F. Käppeler, Astron. Astrophys. **211**, 245 (1989).
[35] J. A. Holmes, S. E. Woosley, W. A. Fowler, and B. A. Zimmerman, At. Data Nucl. Data Tables **18**, 305 (1976).
[36] K. Takahashi and K. Yokoi, At. Data Nucl. Data Tables **36**, 375 (1987).
[37] N. Klay, F. Käppeler, H. Beer, and G. Schatz, Phys. Rev. C **44**, 2839 (1991).
[38] M. Rayet, N. Pranzos, and M. Arnould, Astron. Astrophys. **227**, 271 (1990).
[39] W. M. Howard, B. S. Meyer, and S. E. Woosley, Astrophys. J. **373**, L5 (1991).
[40] R. Gallino, M. Busso, G. Piccino, C. M. Raiteri, and A. Renzini, Astrophys. J. **334**, L45 (1988).
[41] R. Gallino, private communication (1990).
[42] S. Jaag, Diploma thesis, University of Karlsruhe, 1990 (unpublished).
[43] K. Wisshak, W. Schanz, and F. Käppeler (unpublished).

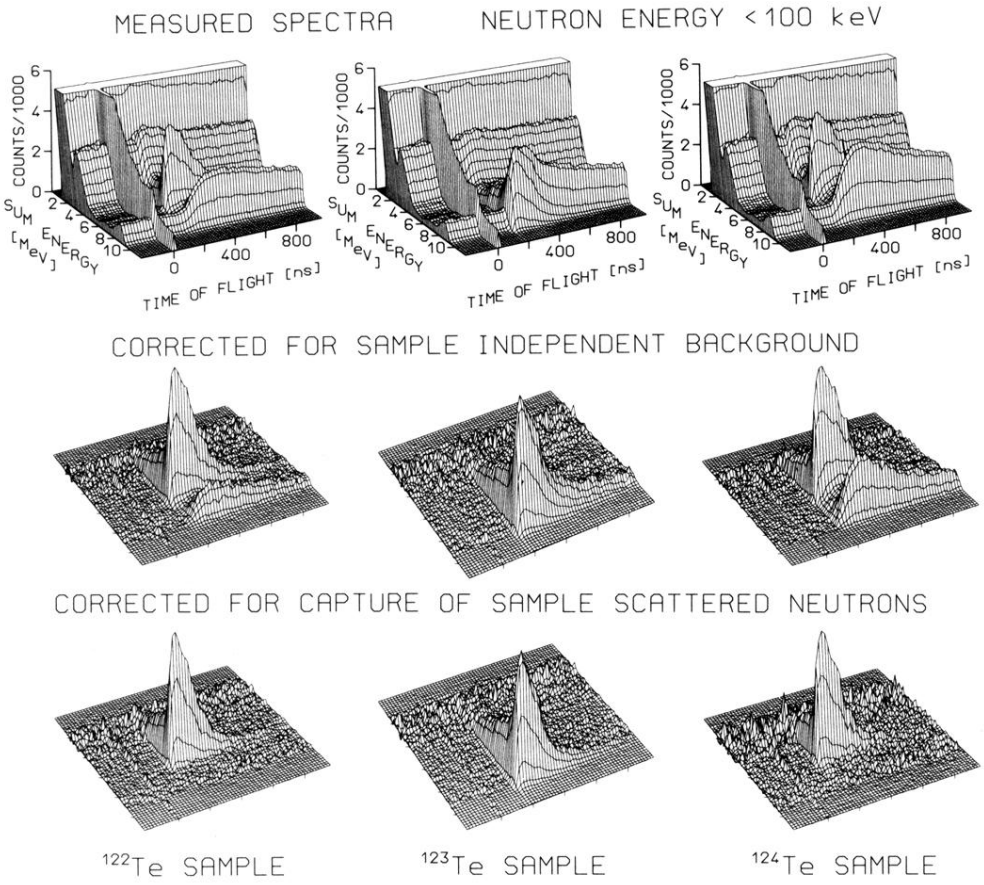

FIG. 2. The different steps of background subtraction in the two-dimensional sum energy vs TOF spectra. Events with multiplicity $m > 2$ are shown for the *s*-only tellurium isotopes measured in the run with 100 keV maximum neutron energy. (The original resolution of 128×2048 channels was compressed in the plots into 64×64 channels.)